Thermally activated resonant grating using a vanadium dioxide waveguide

E. K Koussi, I. Verrier, T. Kämpfe, S. Reynaud, F. Bourquard, D. Jamon, H. Bruhier, Y. Jourlin, O. Parriaux

Research Article | Vol. 11, No. 4 / 1 April 2021 / Optical Materials Express 1093
Optical Materials EXPRESS

Thermally activated resonant grating using a vanadium dioxide waveguide

E. K. KOUSSI, I. VERRIER, T. KÄMPFE,* S. REYNAUD, F. BOURQUARD, D. JAMON, H. BRUHIER, Y. JOURLIN, AND O. PARRIAUX

Université de Lyon, UJM-Saint-Etienne, CNRS, Institut d'Optique Graduate School, Laboratoire Hubert Curien, UMR 5516, F-42023 Saint-Etienne, France
*thomas.kampfe@univ-st-etienne.fr

Abstract: In this work, we report on the design of a one-dimensional subwavelength resonant grating comprised of a fused silica substrate and a bi-layer waveguide, consisting of a solgel synthetized anatase TiO_2 layer followed by a thin VO_2 layer that is applied using pulsed laser deposition and rapid thermal annealing. A TE waveguide mode is excited under normal incidence in the VO_2/TiO_2 bi-layer via a positive photoresist based grating printed on top, leading to high resonant reflection at room temperature. Increasing the temperature to about 68°C causes the VO_2 to undergo a dielectric to metallic transition accompanied by optical modifications in the IR region, canceling the resonance effect. This thermally triggered absorber/emitter tunable configuration enabling the on and off switching of optical resonant excitation in a reversible manner is proposed for passive Q-switching self-protecting devices for high power lasers in the IR wavelength range. Modeling of the optimized temperature dependent resonant waveguide and preliminary experimental results are presented.

1. Introduction

Optical switches induced by electric [1], thermal [2], acoustic [3], or magnetic [4] effects are well known and widely reported. A new generation of simple and cost-effective optical modulators based on smart phase change materials is being developed, notably for use in passive control systems. In this context, VO_2 has been one of the most attractive candidates for realizing an efficient optical switching effect because of the ability to change its optical properties around a transition temperature of ~68°C [5–8], where dielectric to metal transition occurs. At room temperature, VO_2 presents a monoclinic crystal structure while above 68°C the crystal changes to a tetragonal rutile structure [9]. This phase change is evident in the optical response from the near infrared regime down to the terahertz spectral region [10–12]. Thanks to this property, VO_2 is widely exploited in novel plasmonic-based structures. When placed close to a metal, VO_2 can incite surface plasmon resonances, whose efficiency depends on its state being dielectric or metallic. The resonant response can be significantly enhanced by adding a corrugation. Such hybrid structures developed for optical switching are strongly dependent on their optical and geometrical characteristics, allowing to fine-tune the operating wavelength. In particular, structured VO_2 has been used for thermal rectification of radiative diodes and thermal transistors [13,14]. 1D gold gratings, situated on a VO_2 film and a bottom Au layer have been proposed for a temperature dependent excitation of a magnetic resonance [15]. Tunable metamaterial structures realizing a wavelength switch based on 1D periodic VO_2 gratings on MgF_2 and VO_2 films [16] have also been presented. Other applications are super-efficient absorbers based on subwavelength, 1D and 2D patterns [17], infrared absorption amplification for aircrafts [18], thermally triggered grating diffraction efficiency control [19] using Al_2O_3/VO_2 gratings, broadband optical reflectance tuning using $Au/VO_2/Au$ nanowires [20], as well as improved

#413373 https://doi.org/10.1364/OME.413373
Journal © 2021 Received 3 Nov 2020; revised 10 Dec 2020; accepted 10 Dec 2020; published 12 Mar 2021

Optical Materials EXPRESS

absorption efficiency for bolometers based on a $Si_3N_4/VO_2/Si_3N_4$ multilayer structure with a metal grating [21]. Further extensive studies [22,23] were carried out to investigate the influence of structural parameters (grating groove depth and grating line width) on the wavelength tunability of a VO_2 waveguide-mode plasmonic nanograting for optical switching.

Unlike many of the above-mentioned devices that rely on metals for resonant effects, the structure studied here uses a dielectric only system using waveguide excitations for the optical switching, which is additionally fabricable with fairly standard lithographic techniques. This allows theoretically to work with very low absorption, allowing for a tunable, waveguide mode resonance in reflection applicable to passive Q-switching applications in lasers as proposed in [24]. A normally incident TE polarized beam couples to a waveguide mode in the VO_2/TiO_2 bilayer via the grating, inducing a high reflectivity. The VO_2 thermally activated layer is designed to cancel this resonance at elevated temperatures (above 68°C), leading to high transmission. This mechanism allows realizing a passive switch that works solely on thermal activation. A first, switchable demonstrator is fabricated and tested, which although not yet very well conform to the theoretically optimized structure demonstrates the switching effect with a 20-percentage points maximal reflectance change at room temperature in accordance with the simulations.

This paper is organized as follows: Section 2 presents the modeling and design of the structure, including a parametric study. In Section 3, the technological steps are explained and fabricated elements are presented, followed in Section 4 by first results for characterizing the switching effect experimentally. Section 5 concludes the paper.

2. Optical design and simulation

We will first introduce the operational principle of the waveguide resonance followed by an explanation of the switching effect. An optimization of the structure parameters is performed in order to find the most suitable grating design.

2.1. Principle of waveguide resonance and switching effect

The wavelength dependent, resonant structure is comprised of rectangular positive photoresist (PR) ridges of height h, situated on a $d_1 = 25$ nm VO_2 thin film and an anatase TiO_2 layer of thickness d_2, supported by a SiO_2 substrate (Fig. 1).

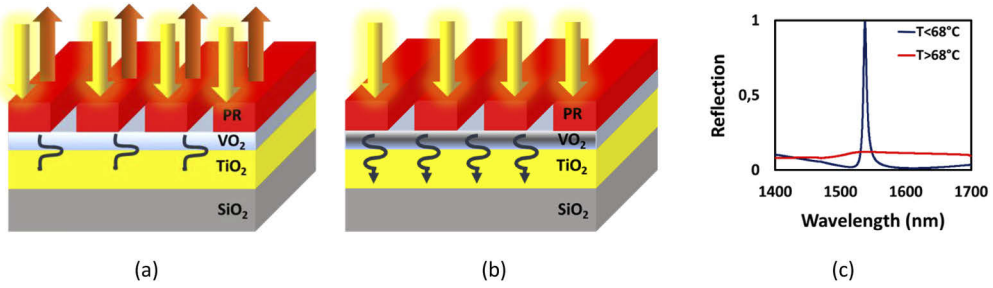

Fig. 1. (a) Schematic representation of the resonant structure in the dielectric phase ($T_{VO_2} < 68$°C) leading to a sharp dielectric reflection resonance under TE polarization (b). The same structure in the metallic phase ($T_{VO_2} > 68$°C), canceling the resonant reflection (c) Example of a reflection spectrum of the resonant structure in the dielectric (cold) state in blue and in the metallic (hot) state in red.

In the presented structure, in order to maximize the efficiency of the resonant reflection (normal incidence, TE polarization) in the cold state, we need to assure a single mode operation of the waveguide bilayer. Therefore, it is essential to adjust the cut-off waveguide thickness w for the

Optical Materials EXPRESS

desired wavelength range of $\lambda_S = 1400$ nm – $\lambda_L = 1700$ nm, using the dispersion equation for the TE mode (setting the effective index n_e of the mode equal to n_s) [25]:

$$\frac{w}{\lambda}|_{cut-off} = \frac{m\pi + \arctan\sqrt{(n_s^2 - n_c^2)/(n_g^2 - n_s^2)}}{2\pi\sqrt{(n_g^2 - n_s^2)}} \tag{1}$$

with n_s, n_c and n_g, being the refractive indices of the substrate, cover and waveguide respectively. Hence, with $m = 0$ and $\lambda_L = 1700$ nm the fundamental mode is maintained and with $\lambda_S = 1400$ nm and $m = 1$ the second mode is excluded. However, the limit for fundamental mode existence needs to satisfy one additional condition. To prevent diffraction orders in the SiO_2 substrate and spurious resonant reflections in the 1700 nm -1400 nm wavelength range, the introduction of the w_{eq} term is essential. The equivalent grating-waveguide thickness w_{eq} is defined as the thickness of a uniform gratingless dielectric waveguide with the permittivity ${n_g}^2$ of the actual waveguide for the TE polarization (Eq. (2)). For a duty cycle of 0.5, the grating-waveguide equivalent thickness w_{eq} [26]:

$$w_{eq} = w_g + h\sqrt{(1 + n_{gg}^2)/2n_g^2} \tag{2}$$

will be set between the cutoff thickness w_{c0} of the fundamental TE_0 mode and the cutoff thickness w_{c1} of the first higher order TE_1 mode, where w_g is the sum of d_1 and d_2 corresponding to the VO_2 and TiO_2 thickness respectively, and h is the thickness of the binary photoresist grating of n_{gg} refractive index. Finally, the TE dispersion equation (Eq. (1)) defines the TE_0 and TE_1 mode cutoff thicknesses w_{c0} and w_{c1}, and gives the range of w_{eq} for single mode operation:

$$\lambda_L \frac{arctan\left[\sqrt{(n_s^2 - n_c^2)/(n_g^2 - n_s^2)}\right]}{2\pi(n_g^2 - n_s^2)^{1/2}} < w_{eq} < \lambda_S \frac{arctan\left[\sqrt{(n_s^2 - 1)/(n_g^2 - n_s^2)} + \pi\right]}{2\pi(n_g^2 - n_s^2)^{1/2}}. \tag{3}$$

The above condition (Eq. (3)) evaluates to 93 nm < w_{eq} < 500 nm for the aforementioned wavelength range. A detailed investigation for the optimal parameters of w_{eq} will follow in the next subsection. For this study, the wavelength of interest is set to $\lambda = 1500$ nm, coinciding with strong material property changes between VO_2 cold and hot state [27]. Numerical simulations were carried out to study the influence of the structural parameters thickness of the TiO_2 layer, VO_2 film thickness, grating width and duty cycle on effect on the resonance behavior.

2.2. Determination of the refractive indices of the layer

The optimization of the resonant reflection of the proposed structure is highly dependent on the VO_2 phase change layer, and thus requires a precise measurement of the refractive index in the different states of the material. Therefore, ellipsometry measurements were performed for a thin VO_2 film deposited on silicon. The resulting, temperature-dependent refractive index and absorption coefficient n and k, displayed in Fig. 2, were deduced from ellipsometric spectra measured from 300 nm to 2000 nm at two distinct temperatures, 25°C and 85°C. The experimental ellipsometric parameters were fitted with a Tauc-Lorentz formula using 3 oscillators ($i = 1..3$) with the usual parameters [28] : ε_∞ (high frequency dielectric constant), E_g (optical band gap), A_i (absorption peak amplitude), E_i (energy of the absorption peak), and C_i (peak broadening terms).

With the measured refractive indices at $\lambda = 1500$ nm and considering the minimum obtained manufactured thickness of VO_2 ($d_1 = 25$ nm), it can be seen that to fulfill the resonant reflection criterion explained above an additional layer adjacent to the VO_2 is necessary (Eq. (3)). TiO_2, which is widely offered for waveguide layers, offers good stability and its refractive index can be

Optical Materials EXPRESS

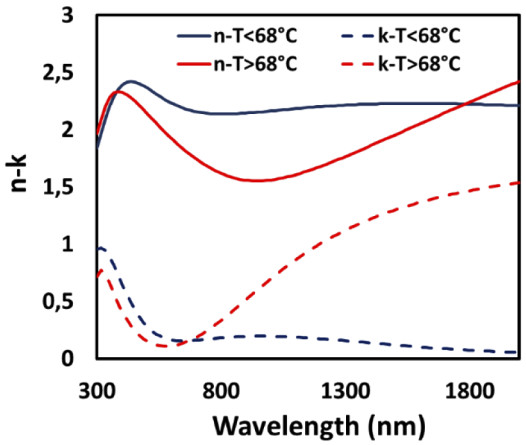

Fig. 2. Refractive index (n) (plain line) and extinction coefficient (k) (dashed line) of vanadium dioxide thin film: cold state (blue) and hot state (red).

adjusted during annealing process. The TiO_2 refractive index is then fixed at 2.2, close to the value of 2.19 of the refractive index of VO_2 at 1500 nm for cold state. The refractive index of the grating photoresist is set to $n_{gg} = 1.67$.

2.3. *Determination of layer thickness, grating depth and width*

This optical simulations of the resonant structure are based on the rigorous wave-optical method RCWA (rigorous coupled wave analysis), using the commercial software "MC Gratings" [29]. The goal is to find for room temperature a highly efficient reflection-resonance under normal incidence for TE polarization at a wavelength of $\lambda = 1500$ nm. For our first tests the period is imposed at $\Lambda = 1$ µm, with the duty cycle (ridge width / period) set to 0.5. The height of the TiO_2 layer is set to $d_2 = 70$ nm, reusing already determined experimental layer height values of previously produced, anatase phase TiO_2 layer. Scanning the VO_2 thickness reveals a peak of

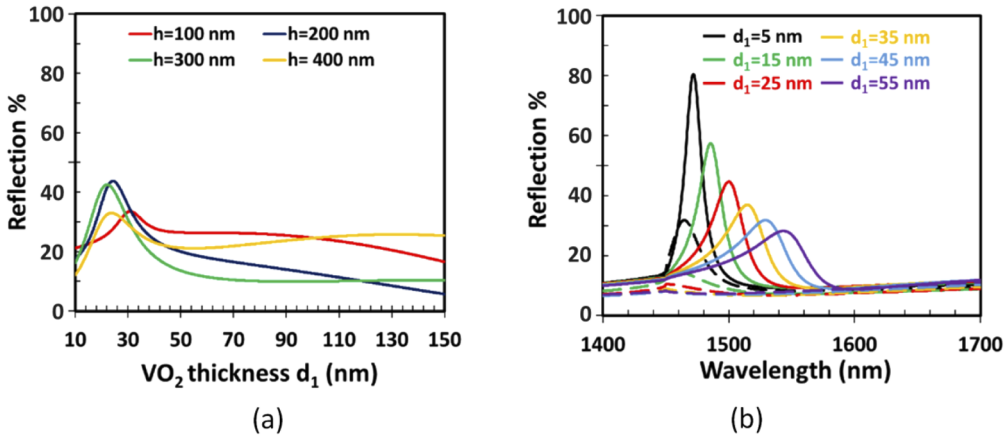

Fig. 3. (a) Reflection at $\lambda = 1500$ nm versus the VO_2 thickness d_1 (cold state) for different photoresist grating depths h ($d_2 = 70$ nm, $\Lambda = 1$ µm and $DC = 0.5$); (b) Reflection versus wavelength at $T < 68$ °C (plane lines) and $T > 68$ °C (dashed lines) for different VO_2 thicknesses d_1 ($h = 200$ nm, $d_2 = 70$ nm, $\Lambda = 1$ µm and $DC = 0.5$).

Optical Materials EXPRESS

the reflection at around $d_1 = 25$ nm in cold state (Fig. 3(a)). Additionally, the grating depth has been varied from $h = 100$ nm to 400 nm in order to optimize the grating-waveguide coupling and increase the maximal reflection value, resulting in an optimal grating height of ~200 nm. The difference in reflection needs to be substantial between the cold and hot state in order to promote the switch effect we are looking for. Looking at the spectral response of our structure it turns out that by decreasing the VO_2 thickness the maximal reflection can be increased further for wavelengths that are slightly smaller than the originally chosen 1500 nm (Fig. 3(b)), while retaining a low reflection in the hot state.

The best response regarding the maximal reflection is obtained for the experimentally minimal possible VO_2 thickness of $d_1 = 5$ nm, reaching about ~ 80% reflection with a ~40 percentage points metallic to insulator (MIT) difference. For $\lambda = 1500$ nm the maximal attainable reflectance drops to ~40% for 25nm VO_2 thickness d_1. In comparison, Thomas *et al.* [20] also reported a 40 percentage points MIT difference for values of $d_1 < 20$ nm thickness of VO_2. Having found a good range of possible VO_2 thicknesses d_1, we now need to determine the optimal value of the photoresist grating depth h. A detailed scan around the previously found optimal value of $h = 200$ nm (Fig. 3(a)) shows a maximal reflection at $h = 216$ nm (Fig. 4(a)). Subsequently, the influence of the TiO_2 layer was reexamined, resulting in an optimal value of $d_2 = 75$ nm (Fig. 4(b)).

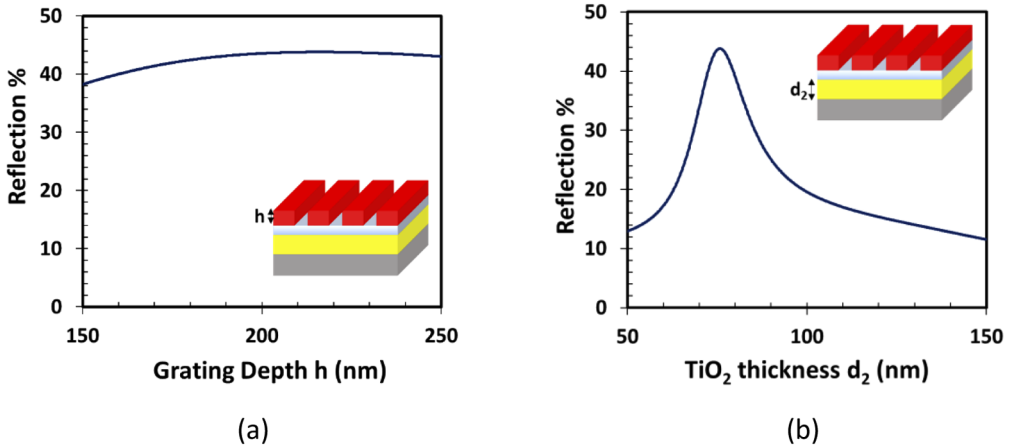

Fig. 4. (a) Reflection scan versus the grating depth h at wavelength $\Lambda = 1500$ nm, with $d_1 = 25$ nm, $d_2 \sim 70$ nm, $\Lambda = 1$ µm and $DC \sim 0.5$; (b) reflection scan versus the TiO_2 thickness d_2 at $\Lambda = 1500$ nm with $h = 216$ nm, $d_1 = 25$ nm, $\Lambda = 1$ µm and DC~0.5.

A change in the spectral shape of the resonance is also observed for a variation of the grating's duty cycle $DC = w / \Lambda$ from 0.2 to 0.7 (Fig. 5(a)), which is due to changing conditions for the coupling into the waveguide mode. The coupling increases with from $DC = 0.2$ to ~0.5, increasing the maximum reflection. The peak is additionally slightly redshifted. When DC increases further, the coupling decreases again, reducing maximum reflection. Analyzing he reflection as a function of DC results in an optimal value of $DC = 0.44$ for $\lambda = 1500$ nm (Fig. 5(b)).

Taking all the numerical optimizations of the structure into account results in an optimal parameter set of $\Lambda = 1$ µm, $DC = 0.44$, $h = 216$ nm, $d_1 = 25$ nm and $d_2 = 75$ nm (Fig. 6(a)). This leads to a value of $w_{eq} = 242$ nm, which respects the initial calculated inequality of 93 nm < w_{eq} < 500 nm for managing the TE_0 propagation mode.

The switching effect, investigated up to this point by numerical optimization mainly, can be better understood by analyzing the electric field distribution inside the grating and the waveguide layer at the resonance wavelength $\lambda = 1500$ nm. Figure 7 shows the electric field in one unit cell of the grating. When the VO_2 is in its dielectric phase (Fig. 7(a)), the structure confines

Optical Materials EXPRESS

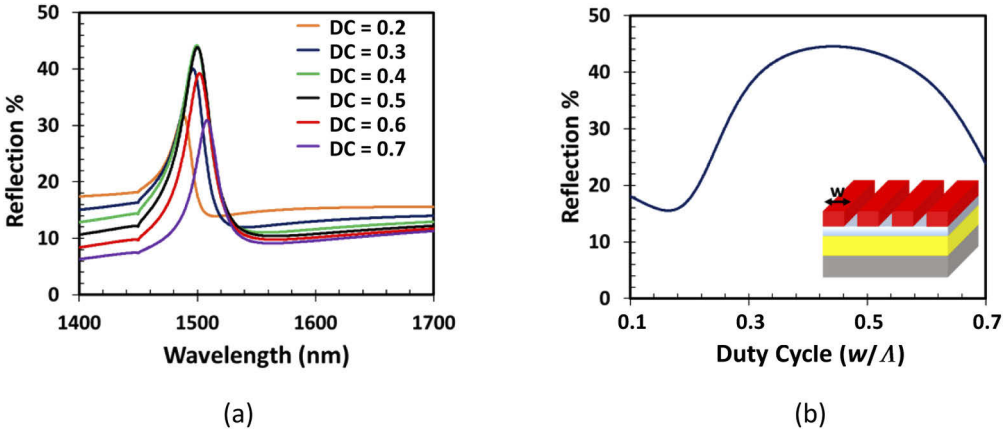

Fig. 5. (a) Effect of a duty cycle variation on the reflection spectrum for $h = 216$ nm, $d_1 = 25$ nm, $d_2 = 75$ nm and $\Lambda = 1$ µm; (b) reflection as a function of the grating's duty cycle at $\lambda = 1500$ nm with $h = 216$ nm, $d_1 = 25$ nm, $d_2 = 75$ nm and $\Lambda = 1$ µm.

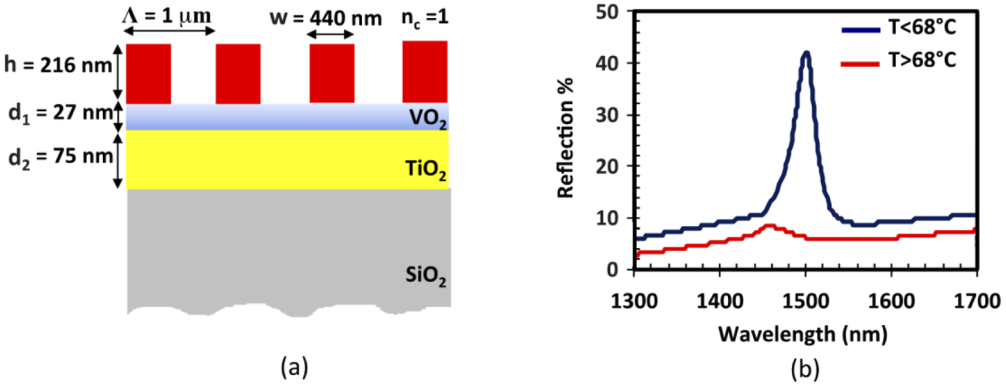

Fig. 6. (a) Final structure for a wavelength resonance at $\lambda = 1500$ nm; (b) spectral response of this configuration for the dielectric and metallic phase.

the electric field strongly within the waveguide layer, resulting in a 4-fold amplification of the incident field amplitude, which demonstrates the strong coupling between the normal incident beam and the fundamental propagating mode in the waveguide. Figure 7(b) shows that changing to the metallic VO_2 phase, thus increasing the imaginary part of its refractive index, leads to a strong absorption of the amplified electric field inside the VO_2 layer. Additionally, the change in the real part of its refractive index for the hot state slightly shifts the resonance condition away from the maximum reflection configuration for cold state in Fig. 7(a). The combination of those effects leads to an almost complete annihilation of the waveguide resonance, leading to a drastically reduced reflection at the resonance wavelength as can be seen in Fig. 6(b).

Optical Materials EXPRESS

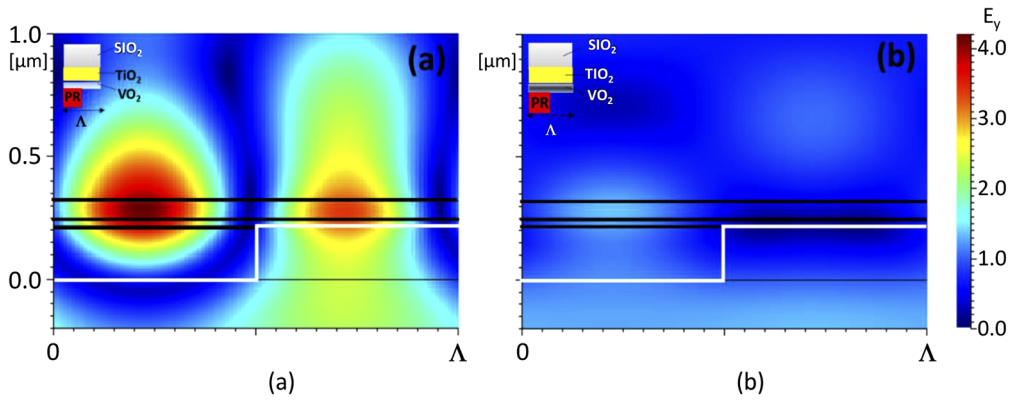

Fig. 7. Distribution of the electric field E_y (relative to the electric field of the incident beam) at the resonance wavelength of $\lambda = 1500$ nm when the VO_2 is (a) in its dielectric phase with $n = 2.23$ and $k = 0.126$, and (b) in its metallic phase with $n = 1.92$ and $k = 1.273$, showing a strong resonant effect for the dielectric phase and almost no resonant behavior for the metallic phase.

3. Fabrication and characterization process

The fabrication process of the resonant structure starts with the TiO_2 and VO_2 layer deposition, followed by a characterization step to check its quality. For the first step of applying the TiO_2 to the substrate, a sol-gel approach is used. The TiO_2 doped sol-gel is deposited using a spin coater at 3000 rpm to obtain the desired original height of 300 nm, followed by an annealing process at 500°C during 3 hours, which forms the anatase phase and reduces the height. Measurements using a profilometer DektakXT confirmed a TiO_2 height of $d_2 = 70$ nm as required after this process.

The VO_2 thin film is grown on the TiO_2 layer by pulsed laser deposition, ablating a pure vanadium metal target on a SiO_2 substrate with a 248 nm KrF excimer laser of 117 mJ laser energy at a laser fluence of 5 J/cm^2 and 10 Hz repetition rate. The chamber is evacuated down to 180×10^{-5} Pa, followed by insertion of O_2 until a 3 Pa pressure level is reached, oxidizing the sample and allowing for a steady deposition rate at around 3 nm/minute allowing to reach the required VO_2 thickness of $d_1 = 25$ nm. The deposition is followed by a rapid thermal annealing post baking process, with a special thermal processor crystallizing the vanadium at 450°C during 2 min with 100 Pa O_2 pressure. The height of the VO_2 layer is measured by SEM using a separate plane Si substrate that was cleaved in order to analyze the profile of the structure (Fig. 8), revealing a homogeneous deposition of a $d_1 = 27$ nm VO_2 layer. The reason for using a separate conducting substrate is that the VO_2 layer is significantly less well resolved in the SEM images of the final bilayer on an SiO_2 substrate (compare with Fig. 10(b)).

For the optical characterization of the bilayer we use an infrared transmission spectrometer with an adapted sample holder consisting of a metal plate connected to a thermocouple and temperature controller (Fig. 9(a)). By heating the sample up to 100°C and subsequently cooling to room temperature, the predicted change in transmission can be observed (Fig. 9(b)), as well as a clear hysteresis for the transmission curve. The optical transmittance change reaches 23.7 percentage points, with an average transition temperature of ~69 °C and a hysteresis width of 14 °C.

After having verified the temperature dependency of the VO_2, the grating was fabricated starting with the deposition of a photoresist layer by spin coating at 3000 rpm. The grating is inscribed in the resist by laser interference lithography using a 442 nm continuous laser that creates a sinusoidal, periodic exposure of the resist with a 1 μm period, followed by a 15

Optical Materials EXPRESS

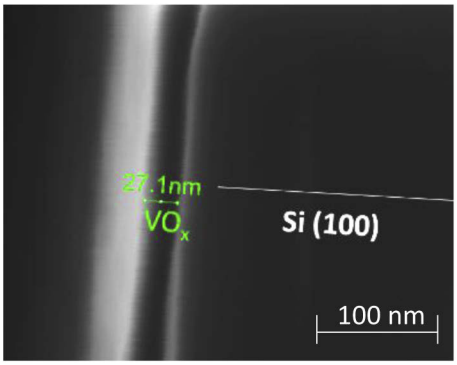

Fig. 8. Cross-section of SEM image in VO_2 thin film deposited on silicon and annealed at 450 °C during 2 min.

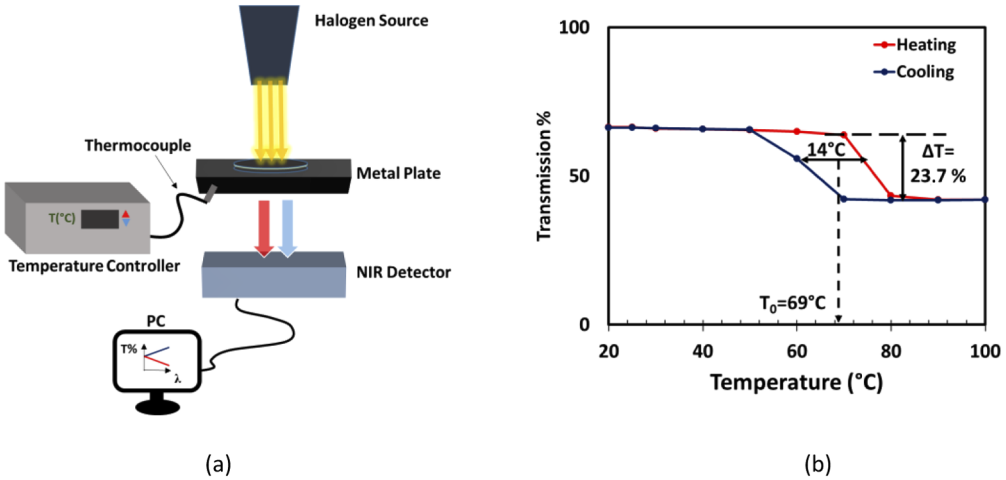

Fig. 9. (a) Set-up for measuring the transmitted spectrum during the heating process and (b) transmission of the bilayer TiO_2/Vo_2 structure (see also Fig. 10) at $\lambda = 1500$ nm versus temperature, showing hysteretic behavior around the transition temperature of 69 °C.

sec development in a basic solution. The obtained gratings were analyzed using AFM scans (Fig. 10(a)) of the surface, as well as SEM images of a cleaved sample (Fig. 10(b)). The measured total height of the waveguide of $d_1 + d_2 = 106$ nm allows to deduce the TiO_2 layer height to be $d_2 = 79$ nm, using the previously determined VO_2 layer height of $d_1 = 27$ nm (Fig. 8).

The SEM and AFM images reveal a sinusoidal grating profile with a period of $\Lambda = 1$ µm and a height of $h \sim 190$ nm. As opposed to the simulated structure, the gratings are not open down to the VO_2 layer and do not have a rectangular profile. Arriving at the correct, binary grating profile is difficult in our case, mainly because of the high reflectivity of the bi-layer setup for the incidence conditions used in the interference lithography setup, which is known to create a non-optimal exposure pattern in the resist. We nevertheless continue the investigation with the obtained structures since they also show a reasonably well temperature-dependent resonant effect and will be presented in the following.

Optical Materials EXPRESS

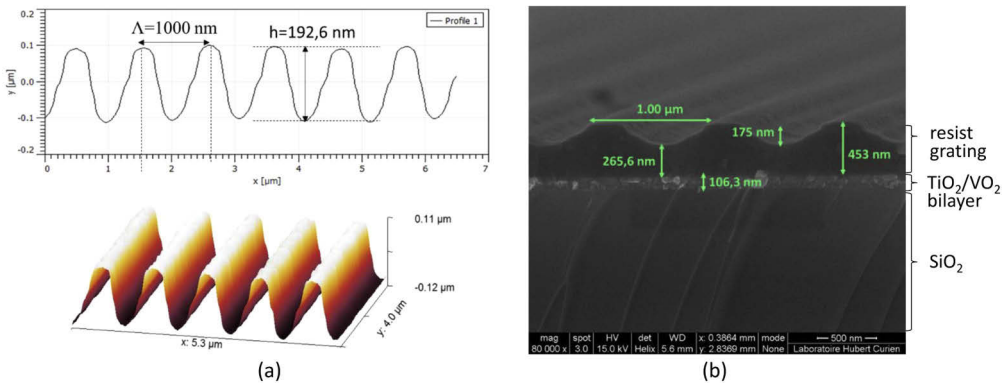

Fig. 10. (a) AFM grating profile measurement and (b) SEM image of a cleaved sample's cross-section.

4. Resonance behavior

The experimental evaluation of the efficiency of the sample was done via spectroscopy with the aforementioned set up in transmission (Fig. 9(a)) and in reflection using this time a 50/50 fiber coupler (Fig. 11), resulting in the reflection and transmission spectra shown in Fig. 12.

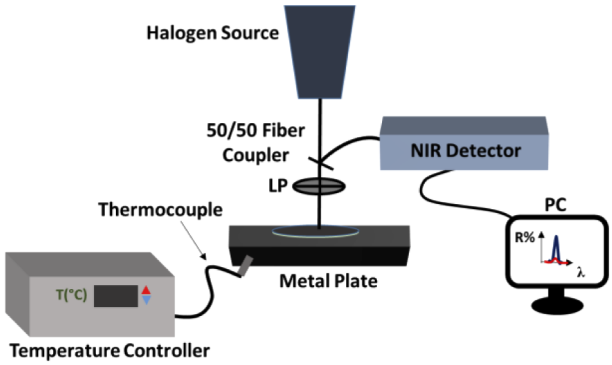

Fig. 11. Set-up for measuring the spectrum in reflection during the heating process.

In order to compare with the theory, the real structural parameters obtained from the SEM and AFM analysis of Fig. 10(b) were used in the simulation. Comparing the resulting spectra (Fig. 12) to the initial simulation of the optimized structure (Fig. 6(a)) reveals a discrepancy that can be attributed to the grating parameter depth h being different from the forecasted one and to the deviation in the profile. The reflection resonance efficiency is thus poorer for the simulation of the real fabricated structure (~10 percentage points instead of 40), whereas the resonance wavelength is unchanged at $\lambda = 1500$ nm.

However, the form of the experimentally obtained curves agrees very well with the simulation for both states, proving that it is possible to thermally switch on and off the resonant behavior. The effect being not very prominent for reflection, we also show the calculated and measured transmission spectra in Fig. 12, exhibiting theoretically a stronger resonance of ~40 percentage points, which is thus easier to measure for this first test setup. The experimental transmission curves allow in this case to clearly identify the resonance in the cold state and its complete elimination in the hot state at the predicted wavelength of $\lambda = 1500$ nm. Reasons for the remaining

Optical Materials EXPRESS

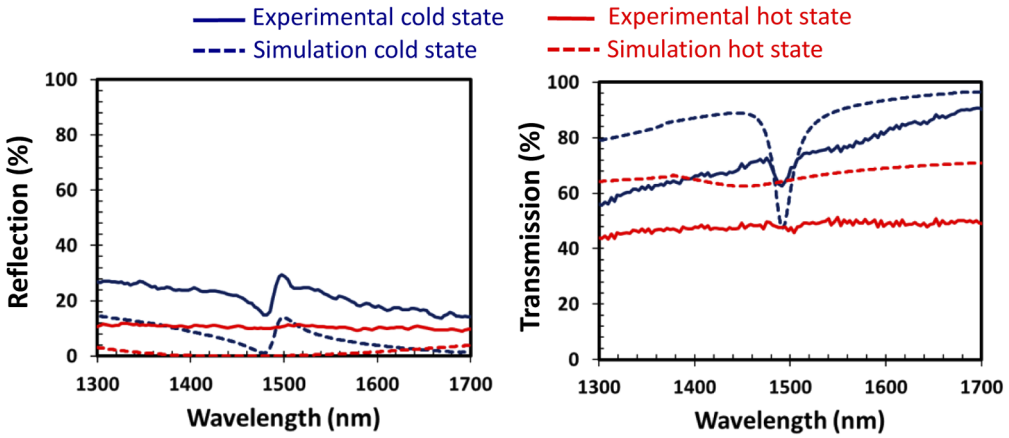

Fig. 12. Measured resonance efficiencies (solid lines) of the structured sample upon heating (>100°C, red lines) and cooling (room temperature, blue lines) in comparison with simulations using the real structural parameters (dashed lines) under normal incidence for TE polarization.

difference in the modulation depth can be the roughness of the VO_2 layer, inducing diffusion losses.

5. Conclusion

In this paper the feasibility of a structure exhibiting a thermal switching behavior based on a VO_2 layer associated with a dielectric resonant grating has been demonstrated. The theoretical optimization shows a good potential for a reversible thermally induced spectral transmission resonance, whereas first experimental results confirm the effect but stay significantly below the expected resonance efficiency due to deviations in the grating parameters for the first experimental realization. It has been shown that the thermally induced switching of the VO_2 from the dielectric to the metallic state can be used to trigger a complete suppression of the resonant reflection effect. One advantage of the approach is the fairly easy fabrication, based solely on a solgel approach, lithographic patterning and PLD deposition, without the need of dry etching steps. In future work we plan to improve the experimental realization of the structure, allowing to make a more thorough optimization taking fabrication limitations as well as other possibly advantageous and fabricable grating shapes (rounded, sinusoidal) into account, leading to a strong, switchable resonant reflection that can be envisioned to be used as optical elements providing a protection against high intensity reflections potentially destroying the cavities of high power IR lasers.

Funding. LabEx MANUTECH-SISE (ANR-10-LABX-0075); Agence Nationale de la Recherche (ANR-11-IDEX-0007).

Disclosures. The authors declare no conflicts of interest.

References

1. Q. Wang and J. Yao, "A high-speed 2×2 electro-optic switch using a polarization modulator," Opt. Express **15**(25), 16500–16505 (2007).
2. X. Fang and L. Yang, "Thermal effect analysis of silicon microring optical switch for on-chip interconnect," J. Semicond. **38**(10), 104004 (2017).
3. D. A. Smith, R. S. Chakravarthy, Z. Bao, J. E. Baran, J. L. Jackel, A. d'Alessandro, D. J. Fritz, S. H. Huang, X. Y. Zou, S. M. Hwang, A. E. Willner, and K. D. Li, "Evolution of the acousto-optic wavelength routing switch," J. Lightwave Technol. **14**(6), 1005–1019 (1996).

Optical Materials EXPRESS

4. S. O'Brien, D. McPeake, S.A. Ramakrishna, and J.B Pendry, "Near-infrared photonic band gaps and nonlinear effects in negative magnetic metamaterials," Phys. Rev. B. **69**(24), 241101 (2004).
5. S. Westman, I. Lindqvist, B. Sparrman, G.B. Nielsen, H. Nord, and A. Jart, "Note on a Phase Transition in VO_2," Acta Chem. Scand. Available from: https://www.osti.gov/biblio/4014769 (1989) [Internet]. 1961 Jan 1 [cited 2019 Oct 14]; 15.
6. T. Kawakubo and T. Nakagawa, "Phase Transition in VO_2," J. Phys. Soc. Jpn. **19**(4), 517–519 (1964).
7. T. Mitsuishi, "On the Phase Transformation of VO_2," Jpn. J. Appl. Phys. **6**(9), 1060–1071 (1967).
8. C. N. Berglund and H. J. Guggenheim, "Electronic Properties of VO_2 near the Semiconductor-Metal Transition," Phys. Rev. **185**(3), 1022–1033 (1969).
9. L. Whittaker, C. J. Patridge, and S. Banerjee, "Microscopic and Nanoscale Perspective of the Metal−Insulator Phase Transitions of VO_2: Some New Twists to an Old Tale," J. Phys. Chem. Lett. **2**(7), 745–758 (2011).
10. Y. Gao, H. Luo, Z. Zhang, L. Kang, Z. Chen, J. Du, M. Kanehira, and C. Cao, "Nanoceramic VO_2 thermochromic smart glass: A review on progress in solution processing," Nano Energy **1**(2), 221–246 (2012).
11. M. F. Becker, A. B. Buckman, R. M. Walser, T. Lépine, P. Georges, and A. Brun, "Femtosecond laser excitation of the semiconductor metal phase transition in VO_2," Appl. Phys. Lett. **65**(12), 1507–1509 (1994).
12. M. Beck, D. Hofstetter, T. Aellen, J. Faist, U. Oesterle, M. Ilegems, and H. Melchior, "Continuous Wave Operation of a Mid-Infrared Semiconductor Laser at Room Temperature," Science **295**(5553), 301–305 (2002).
13. A. Ghanekar, Y. Tian, M. Ricci, S. Zhang, O. Gregory, and Y. Zheng, "Near-field thermal rectification devices using phase change periodic nanostructure," Opt. Express **26**(2), A209–218 (2018).
14. J. Liang, J. Guo, Y. Zhao, Y. Zhang, and T. Su, "Localized surface plasmon resonance modulation of totally encapsulated VO_2/Au/VO_2 composite structure," Nanotechnology **29**(27), 275710 (2018).
15. H. Wang, Y. Yang, and L. Wang, "Switchable wavelength-selective and diffuse metamaterial absorber/emitter with a phase transition spacer layer," Appl. Phys. Lett. **105**(7), 071907 (2014)..
16. H. Wang, Y. Yang, and L. Wang, "Wavelength-tunable infrared metamaterial by tailoring magnetic resonance condition with VO_2 phase transition," J. Appl. Phys. **116**(12), 123503 (2014)..
17. Z. Liu, M. Zhao, J. Gao, Y. Li, and S. Jiang, "Thermally tunable broadband omnidirectional and polarization-independent super absorber using phase change material VO_2," Results Phys. **7**, 4222–4225 (2017).
18. K. Sun, C. A. Riedel, A. Urbani, M. Simeoni, S. Mengali, M. Zalkovskij, B. Bilenberg, C. H. de Groot, and O. L. Muskens, "VO_2 Thermochromic Metamaterial-Based Smart Optical Solar Reflector," ACS Photonics **5**(6), 2280–2286 (2018).
19. S. J. Kim, S. Choi, C. Choi, Y. Lee, J. Sung, H. Yun, J. Jeong, S. Eun Mun, Y. Wook Lee, and B. Lee, "Broadband efficient modulation of light transmission with high contrast using reconfigurable VO_2 diffraction grating," Opt. Express **26**(26), 34641–34654 (2018).
20. A. Thomas, P. Savaliya, K. Kumar, A. Ninawe, and A. Dhawan, "Au nanowire-VO_2 spacer-Au film based optical switches," J. Opt. Soc. Am. B **35**(7), 1687–1697 (2018).
21. Y.F. Zhang, Y. Wang, Y.Q. Wu, C.M. Liu, X.D. Lu, and T. Zhou, "Study on Improving the Absorption Efficiency of Uncooled Infrared Sensor by Using Grating," DEStech Trans. Comput. Sci. Eng. [Internet]. 2018 [cited 2019 Oct 22]; 0(cmsms). Available from: http://www.dpi-proceedings.com/index.php/dtcse/article/view/25257
22. Y. Sharma, V. A. Tiruveedhula, J. F. Muth, and A. Dhawan, "VO_2 based waveguide-mode plasmonic nano-gratings for optical switching," Opt. Express **23**(5), 5822–5849 (2015).
23. J. Jeong, A. Joushaghani, S. Paradis, D. Alain, and J. K. S. Poon, "Electrically controllable extraordinary optical transmission in gold gratings on vanadium dioxide," Opt. Lett. **40**(19), 4408–4411 (2015).
24. S. A. Pollack, D. B. Chang, F. A. Chudnovky, and I. A. Khakhaev, "Passive Q switching and mode-locking of Er: glass lasers using VO_2 mirrors," J. Appl. Phys. **78**(6), 3592–3599 (1995).
25. D. Marcuse, "Theory of dielectric optical waveguides," Academic Press, New York, 1974
26. R. Halir, P. J. Bock, P. Cheben, A. Ortega-Moñux, C. Alonso-Ramos, J. H. Schmid, J. Lapointe, D.-X. Xu, J. Gonzalo Wangüemert-Pérez, I. Molina-Fernàndez, and S. Janz, "Waveguide sub-wavelength structures: a review of principles and applications," Laser Photonics Rev. **9**(1), 25–49 (2015).
27. V. Melnik, I. Khatsevych, V. Kladko, A. Kuchuk, V. Nikirin, and B. Romanyuk, "Low-temperature method for thermochromic high ordered VO_2 phase formation," Mater. Lett. **68**, 215–217 (2012).
28. G.E. Jellison Jr. and F.A. Modine, Appl. Phys. Lett. 69, 371 (1996), erratum G.E. Jellison Jr. and F.A. Modine, Appl. Phys. Lett. 69, 2137 (1996).
29. Modal and C Methods Grating Software, available from: https://mcgrating.com/ [cited 9th July 2019].